MRI Estimation of the Arterial Input Function in Mice[1]

Stephen Pickup, PhD, Rong Zhou, PhD, Jerry Glickson, PhD

Rational and Objectives. Dynamic contrast-enhanced (DCE) MRI offers the potential to provide quantitative maps of tumor perfusion parameters and is therefore expected to play an important role in the study of cancer in small animal models. Extraction of such information from DCE-MRI data requires a methodology for determination of the arterial input function (AIF) for the target tissues. An MRI based method for observation of the AIF in a mouse model is demonstrated in the present report.

Materials and Methods. A series of short-axis cardiac images was acquired during the first pass of a bolus of Gadodiamide using a low-resolution, EEG-gated, saturation-recovery gradient echo imaging sequence. The AIF was then extracted from the observed signal intensity changes in the left ventricle (LV) blood pool.

Results. The proposed technique provides sufficient temporal and spatial resolution to accurately characterize the AIF of Gadodiamide in mouse models. The AIF was observed in 4 mice and was found to be qualitatively similar to that previously observed in larger animals. However, significant inter-animal variability in the precise form of the AIF was evident.

Conclusions. The proposed method for determination of AIF in mice has been shown to be effective and reliable. The inter-animal variability observed in the present study suggests that the AIF should be measured in each animal undergoing analysis by DCE-MRI.

Key Words. Arterial input function; dynamic contrast-enhanced MRI; perfusion; vascular permeability; mouse; relaxivity.

Dynamic contrast-enhanced (DCE) MRI has the potential to play an important role in cancer research in small animal models. These methods use fast imaging techniques to monitor the signal changes during the first pass of an IV bolus of a suitable contrast agent (CA). Fitting of the observed changes in signal intensity to a suitable pharmacokinetic model yields quantitative measures of perfusion and/or vascular permeability within various tissues. The pharmacokinetic models most commonly employed for analysis of DCE-MRI data require knowledge of the time-dependent tracer concentration in the vessels feeding the tumor, known as the arterial input function (AIF) (1–3).

The AIF has previously been determined in humans and large animals by sampling arterial blood at multiple time points following tracer administration (4). However, sampling methods simply cannot be implemented in small animals because of the limited blood volume and high heart rates. MRI methods for determining the AIF have also been demonstrated in humans. These techniques extract the AIF from signal intensity changes observed in the blood of the left ventricle (LV) (5) or in large arteries (6) following injection of a CA bolus.

Although several DCE-MRI studies of tumor perfusion in mice have been reported (7–9), relatively few measurements of the AIF in small animal models have been made to date. Evelhoch et al have measured the ^2H_2O AIF in rats by

Acad Radiol 2003; 10:963–968

[1] From the Department of Radiology, University of Pennsylvania, B1 Stellar Chance Laboratories, 422 Curie Blvd., Philadelphia, PA 19104. Received June 9, 2003; revision requested June 17; revised received June 18; revision accepted June 19. Supported by the National Institutes of Health (R24 CA83105 to J.D.G). **Address correspondence to** R.Z.

doi:10.1016/S1076-6332(03)00291-5

shunting blood from the carotid artery through an RF transceiver coil and then back into the rat (10). This approach yielded a precise representation of the AIF, but is obviously invasive. The technique would be very difficult to implement in mice because of the small vessel size. Artemov et al. (11) have had some success in measuring the AIF in mice by wrapping a transceiver coil around the tail. However, this technique offers very low temporal resolution.

In the present report an MRI method for estimation of the AIF in mice is shown. Here, in analogy to the previously reported work in humans (5), the AIF is extracted from the signal intensity changes in the LV blood pool following injection of a bolus of CA.

MATERIALS AND METHODS

Animal Preparation

The animal protocol was approved by the Institute Animal Care and Use Committee (IACUC) at the University of Pennsylvania. Female 6–9-week-old C3H/HEJ mice (National Cancer Institute, Bethesda, MD) were prepared for imaging by inserting a tail vein catheter. The catheter was attached to a piece polyethylene (PE) tubing of sufficient length to extend outside the magnet during imaging. The PE tubing was filled with a solution of CA before attachment to the catheter. The animal was sedated with 1% isoflurane in air at a flow rate of 0.8 L/min through a nose cone. A thermister for monitoring core body temperature was placed rectally and a pair of sub-dermal needle electrodes was placed in the front paws for monitoring the electrocardiogram (ECG). ECG monitoring and gating was accomplished with an MR-compatible small animal vital sign monitor (SA Instruments, Bayshore, NY). This device also regulated a home-built warm air source to maintain the animal's core temperature at 37°C (± 0.2°C) during the imaging protocol. Under these conditions, heart rates were typically in the range of 480–540 beats per minute.

MR Imaging

All MR experiments were performed with a Unity INOVA console (Varian Inc., Palo Alto, CA) equipped with a 4.7 T horizontal bore magnet and a 12 cm gradient insert capable of generating magnetic field gradients of up to 25 G/cm. A home-built 4.5 × 9 cm linearly polarized birdcage RF coil was used for all studies. All MR acquisitions were gated on the R-wave generated by the ECG monitor described above. A delay of 5–10 milliseconds was inserted between the detection of R-wave and initiation of imaging so that image acquisition occurred at end-diastole, when the heart is in the fully dilated state to minimize flow effects.

A single short-axis heart image located well below the mitral valve was selected to avoid turbulence in the blood pool around the valve. A pre-contrast longitudinal relaxation time, T_{10}, map was then generated using the TOMROP (T One by Multiple Read Out Pulses) (12, 13) sequence with TE = 2.2 milliseconds, TI (inversion time) = 4 heartbeats (~480 ms), number of TI intervals = 25, flip angle = 10°, FOV= 2.5 cm, 64 phase encodes, and thk = 1 mm. The sequence used a 90_x-180_y-90_x composite inversion pulse, which was shown to achieve accurate inversion over the entire animal when used in combination with the slightly oversized RF coil.

On completion of the T_{10} mapping protocol, sixty single average, low-resolution (16 phase encodes) images were acquired from the same slice using an ECG-gated saturation-recovery GRE sequence (TE = 2.2 ms, TR = 6 ms, flip angle = 90°, TS = 1 heartbeat-TR). The pulse sequence used a composite saturation pulse (14) to compensate for B_1 inhomogeneity and to ensure complete saturation of the entire blood pool. The saturation pulse was followed by a 5-millisecond 2 G/cm crusher pulse. This protocol yielded a temporal resolution of approximately 2 s/image. A 0.1-mL bolus of 10 mM Gadodiamide (Omniscan; Nycomed Inc., Princeton, NJ) in saline was injected IV in 2 seconds starting after the acquisition of 20 pre-contrast images. A second series of 120 images using identical timing parameters and 2 averages (temporal resolution approximately 4 s/image) was initiated immediately after completion of the first series.

Image Processing

The signal intensity in a saturation-recovery experiment may be expressed by

$$S = A[1 - \exp\{-TS\,R_1\}] \qquad (1)$$

where TS is the saturation-recovery time (1 heartbeat minus TR); $R_1 = 1/T_1$ is the longitudinal relaxation rate constant; and A is a proportionality constant that accounts for transverse relaxation effects, receiver gain, and proton density. The above relation can easily be rearranged to express the relaxation rate constant as a function of the signal intensity as shown below

$$R_1 = -\frac{\ln[1 - S/A]}{TS} \qquad (2)$$

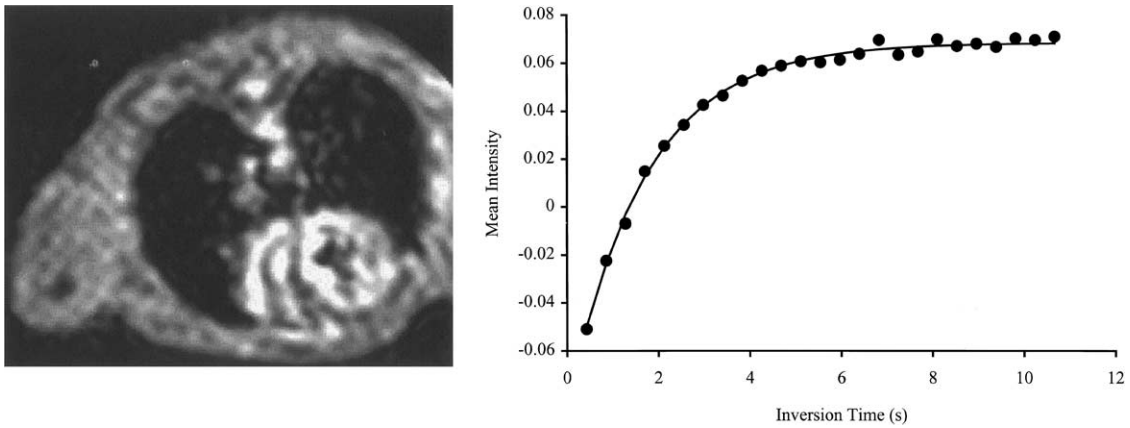

Figure 1. A typical image from the TOMROP protocol **(a)** has high *s/n* and no evidence artifacts due to motion or flow. The signal recovery in a ROI centrally located in the LV is well represented by the least squares three-parameter fit, solid line **(b)**.

In DCE imaging, the R_1 of the blood pool is made time dependent by IV injection of a CA bolus. The relaxation rate in homogeneous systems is known to be proportional to the concentration of CA as expressed by

$$R_1 = R_{10} + r_1 C(t) \qquad (3)$$

where R_{10} ($=1/T_{10}$) is the relaxation rate in the absence of the CA, $C(t)$ is the time-dependent concentration of the CA and r_1 is a constant for a given CA known as the relaxivity. A combination of equations [2] and [3] allows for the determination of the time-dependent concentration of the CA if the parameters A, R_{10}, and r_1 are known.

The value of R_{10} was determined in the TOMROP study. The read pulses in the TOMROP sequence were assumed to have no effect on the axial magnetization of LV blood because most of the blood in the LV is replaced between consecutive read pulses (4 heartbeats). The ejection fraction of the mouse LV under the conditions used in this study has previously been shown to be approximately 65%–75% (15). At this rate the residual blood in the LV after four heartbeats that has "seen" the previous read pulse is ≤1.5% of the total LV volume. Consequently, any saturating effect of the consecutive read pulses can be ignored. The signal intensity of each pixel in the TOMROP images was fit to an exponential recovery using a nonlinear least squares method developed in the interactive data language (IDL) environment (Research Systems, Inc., Boulder, CO) for this purpose. The mean value in an ROI placed at the center of the LV lumen in the resulting T_{10} map was used to generate the value of R_{10} to be used for the analysis of the dynamic data.

The ROI used to determine the R_{10} value was also used to extract mean signal intensities from the dynamic image series. The value of the proportionality constant, A, was determined by substitution of the signal intensity before CA arrival and the previously determined R_{10} value into equation [1]. The resulting $R_1(t)$ data from blood was converted to CA blood concentration, C_b(t), using Eq. [3], and then to plasma concentration *via* the relation C_p(t) = C_b(t)/*(1-Hct)*where *Hct* is the hematocrit. The literature values for r_1 = 4.0 (16) and *Hct* = 0.5 were assumed in the analysis.

The decaying component AIF was fit to a bi-exponential decay of the form

$$C_p(t) = a_f \exp\{(t - t_0)k_f\} + a_s \exp\{(t - t_0)k_s\} \qquad (4)$$

as suggested by Tofts et al. (3) to facilitate a comparison between different AIF measurements. The subscripts *f* and *s* in the above relation identify the fast and slow components of the decay, respectively. The variables a_i and k_i are the amplitudes and decay rates for the *i* component, respectively, and t_0 is the time corresponding to the maximum in the C_p curve. Only data for time $t \geq t_0$ were used in the analysis. A non-linear least squares analysis similar to that used in the generation of the T_1 maps was used to fit the AIF.

RESULTS

A typical image from the TOMROP protocol is depicted in Figure 1a. This is the last image in the inversion

recovery series and as such it shows T_1 weighting. The image has good *s*/*n* and the resolution is sufficient to resolve the ventricles. There is no evidence of cardiac motion or artifacts due to turbulent flow of blood within the LV. All of these factors are indicative of accurate and reliable ECG gating. A ROI was selected in the central region of the LV and the mean signal over this ROI is plotted in Figure 1b as a function of inversion recovery time for the entire TOMROP series. Clearly the full recovery of the axial magnetization is well sampled by the protocol. The solid line in the figure is the least squares three-parameter fit of the experimental data. The quality of the fit is very good over the entire recovery path and there are no systematic errors evident. These observations suggest an accurate and reliable T_1 estimation.

The calculated T_{10} map generated from this data is shown in Figure 2 where the units of the gray scale in the figure are seconds. As is evident in the figure the T_1 of the blood in the ventricles is slightly higher than that of myocardium. The relaxation times of ventricular blood measured in the present study ranged from 1.70 to 1.85 seconds.

A series of images from a DCE study is shown in Figure 3. The images show heavy T_1 weighting and the blood in the ventricles appears hyper-intense. The spatial resolution is limited by the need for high temporal resolution in the AIF data and the need to freeze cardiac motion. The images shown in the figure were generated with only 16 lines of phase encoding as described above. Though poor, the spatial resolution is sufficient to resolve the boundaries of the LV wall.

The time between acquisitions of each frame shown in the figure is approximately 2 seconds. The tail vein injection occurred during the acquisition of the third frame in the figure. The bolus arrives in the LV approximate 6 seconds after completion of the injection as evidenced by the sharp increase in signal intensity in the LV. The rise to maximum intensity in the LV is very rapid, occurring in a period of time comparable to the temporal resolution of the protocol. The decay following the maximum intensity is more gradual and hardly perceptible in the image series.

The mean signal intensity in an ROI placed in the LV blood pool was used to calculate the time-dependent concentration of CA in the plasma, C_p, which is plotted as a function of time in Figure 4. A relatively small ROI centrally located in the LV was selected for this analysis to avoid partial volume averaging near the LV boundaries in the low-resolution images. The plot has the same general

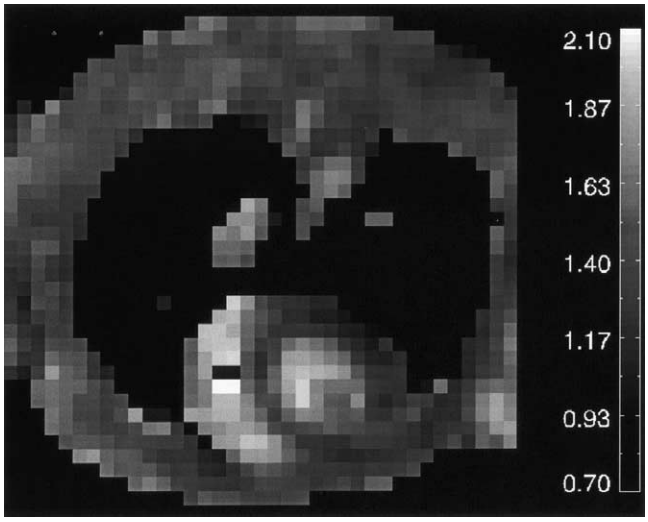

Figure 2. The T_1 map calculated from the TOMROP data typically shows high signal-to-noise and the resolution is sufficient to resolve both ventricles.

form as previously reported AIFs. The C_p is initially zero and increases sharply on the arrival of the bolus in the LV. The temporal resolution of the DCE protocol is such that this transition is sampled by only one or two points. The rapid increase is followed by a gradual two-component decay. In some cases, a spike is observed in the AIF approximately 10–15 seconds after the initial increase in C_p due to recirculation of the bolus front. This spike is not evident in the data shown in the figure.

The solid line shown in the figure is the result of a least squares fit of the data to equation [4]. The overall fit is good; however some systematic error is evident particularly in the transition region between the fast and slow components of the decay. This error suggests a limitation in the model used to derive equation [4], which ignores the contribution of recirculation effects. Other functional forms have been used to model the AIF and often provide better fits. However these forms generally have no theoretical basis and as such the resulting parameters cannot be related to physiology. These models have therefore been avoided in the present analysis.

The DCE protocol was applied to 4 animals and the parameters from fitting of the AIF and T_1 measurements are summarized in the Table. Also shown in the table are the mean values and standard deviations for each of the parameters listed. It is evident in the table that the pre-CA relaxation time for blood is relatively consistent within this small group of animals. However, significant inter-animal variability is evident in the parameter values listed in the table.

Figure 3. A series of images from a DCE study is shown. The series begins before bolus injection and continues through passage of the maximum in the AIF. The temporal resolution of each image in the series is 2 seconds.

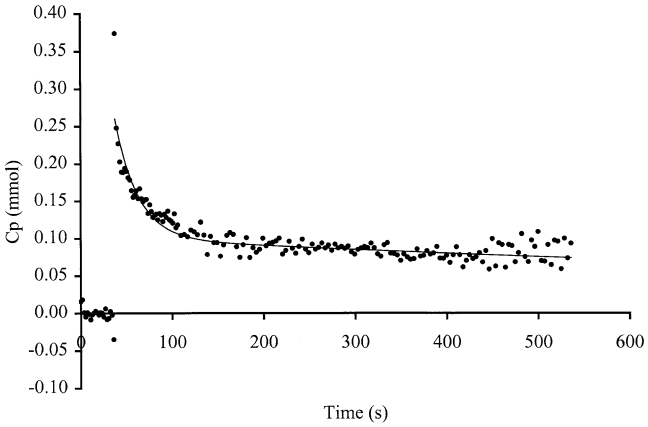

Figure 4. The instantaneous CA concentration in plasma is plotted as a function of time during the passage of the bolus. The solid line in the figure is the result of a least squares fit of the experimental data to a bi-exponential decay.

This inter-subject variability is consistent with previous AIF measurements in humans (5). This variability suggests that the AIF should be measured for each subject rather than assuming a simple functional form for all subjects as is often done in DCE studies.

The slowly decaying component in equation [4] can be roughly identified with the clearance of the contrast agent by the renal system. The parameter a_s is thus an approximation of the concentration of the CA in the plasma after it has been distributed in the animal. Dilution of the bolus delivered in this study into a blood volume that is reasonable for the animal under study, 2 mL, yields a concentration of 0.5 mM. This is the CA concentration that would be observed if it all remained in the plasma and as such represents an upper limit for the value of a_s. The lower limit for this parameter is the concentration of the bolus when it is evenly distributed throughout the body of an animal. Assuming a body volume of 25 mL yields a value of 0.04 mM for the lower limit. All of the values for a_s listed in the table fall in the upper range of these limits.

An approximate value for the a_s parameter is given by calculating the concentration of bolus when it is diluted into the volume accessible to the CA. The CA is known to enter the interstitial space but not enter the cells. The CA therefore has access to only approximately 30% (v/w) (blood = 10%, extra-cellular extra-vascular space = 20%) of animal body weight. Dilution of the bolus into a volume of 30% of the body volume yields an approximate value of $a_s = 0.13$ mM. The values listed in the table are remarkably consistent with this very crude estimate.

The decay rate for the slow component in the AIF is qualitatively related to the half-life of the CA in the animal. The literature provided by the vendor for the CA indicates that the elimination half-life in humans is 77.8 minutes. The half-life of GdDTPA in rats has been reported to be 20 minutes (22). These data translate into decay rates of $k_s = 0.21 \times 10^{-3}$ s^{-1} and 0.83×10^{-3} s^{-1} for humans and rats, respectively. Extrapolation of these data based on animal weight suggests a decay rate of approximately 3×10^{-3} s^{-1} in mice. The values listed in the table are of the correct order of magnitude but are slightly lower than expected based on the above analysis. This difference may suggest a slower than projected renal excretion of CA in mice or may be due to the limited number of animals used in the present study.

DISCUSSION

We have shown a method for estimating the AIF for Gadodiamide in mice by observation of signal intensity changes in the blood pool of the LV during the first pass of a bolus of CA. This method can be incorporated into DCE perfusion studies for tissues that can be visualized in the short-axis cardiac image for simultaneous acquisition of the AIF and tissue perfusion data (21). The spatial resolution of the method is poor but sufficient to allow for accurate quantification of the AIF. The spatial resolution of rapid cardiac images can be significantly improved by application of keyhole filling techniques (17) to the low-resolution images. However this approach was found

Table 1
Dynamic contrast enhanced MRI protocol and the parameters from fitting of the AIF and T_1 measurements as applied to 4 animals

	T_{10} (s)	a_f (mM)	k_f (s^{-1})	a_s (mM)	$k_s \times 10^3$ (s^{-1})
Mouse 1	1.80	0.19	0.027	0.080	0.36
Mouse 2	1.85	0.15	0.11	0.050	2.2
Mouse 3	1.70	0.25	0.10	0.17	1.0
Mouse 4	1.78	0.16	0.04	0.10	0.66
Mean ± S.D.	1.78 ± 0.06	0.19 ± 0.04	0.069 ± 0.042	0.10 ± 0.056	1.05 ± 0.81

to have an unpredictable impact on the signal intensity of the LV blood and therefore was not used in the AIF analysis. A more viable approach to increasing the resolution of the proposed method is the application of parallel imaging techniques, ie, SMASH (18,19) and SENSE (20). These techniques offer potential improvements in the spatial resolution by a factor of 2–4 with no loss in the temporal resolution. The development of parallel acquisition methods in DCE imaging of mouse models is the subject of ongoing development.

The proposed method has been applied to 4 mice and the decaying portion of the AIF has been fit to a bi-exponential decay. The slow component of this decay is known to be qualitatively related to the clearance of the CA by the renal system. The parameters for the slowly decaying component of the AIF generated in the present study were found to be consistent with estimates of these parameters based on the volume available to the CA in the animals and the known half-life of the CA.

The results from the limited number of animals studied here indicate that there is considerable inter-animal variability in the precise form of the AIF. This observation suggests that use of a general model for the AIF, as is frequently done in DCE studies in mice, will lead to significant errors in the estimation of the perfusion parameters. Direct measurement of the AIF using a method similar to that proposed in the present article should therefore be performed to avoid such errors.

REFERENCES

1. Larsson HBW, Stubgaard M, Frederiksen JL, et al. Quantitation of blood–brain barrier defect by magnetic resonance imaging and gadolinium-DTPA in patients with multiple sclerosis and brain tumors. Magn Reson Med 1990; 16:117–131.
2. Brix G, Semmler W, Port R, et al. Pharmacokinetic parameters in CNS Gd-DTPA enhanced MR imaging. J Comput Asst Tomog 1991; 15: 621–628.
3. Tofts PS, Kermode AG. Measurement of the blood–brain barrier permeability and leakage space using dynamic MR imaging. 1. Fundamental concepts. Magn Reson Med 1991; 17:357–367.
4. Weinmann HJ, Laniado M-, Mutzel W. Pharmacokinetic of GdDTPA/dimeglumine after intravenous injection into healthy volunteers. Physiol Chem Phys Med NMR 1984; 16:167–172.
5. Port RE, Knopp MV, Brix G. Dynamic contrast-enhanced MRI using Gd-DTPA: interindividual variability of the arterial input function and consequences for the assessment of kinetics in tumors. Magn Reson Med 2001; 45:1030–1038.
6. Fritz-Hansen T, Rostrup E, Larsson HB, et al. Measurement of the arterial concentration of Gd-DTPA using MRI: a step toward quantitative perfusion imaging. Magn Reson Med 1996; 36:225–231.
7. Bhujwalla ZM, Artemov D, Glockner J. Tumor angiogenesis, vascularization, and contrast-enhanced magnetic resonance imaging. Magn Reson Imag 1999; 10:92–103.
8. Bogin L, Margalit R, Mispelter J, et al. Parametric imaging of tumor perfusion using flow- and permeability-limited tracers. J Magn Reson Imag 2002; 16:289–299.
9. Degani H, Gusis V, Weinstein D, et al. Mapping pathophysiological features of breast tumors by MRI at high spatial resolution. Nature Med 1997; 3:780–782.
10. Simpson NE, He Z, Evelhoch JL. Deuterium NMR tissue perfusion measurements using the tracer uptake approach: I. Optimization of methods. Magn Reson Imag 1999; 42:42–52.
11. Artemov D, Bhujwalla ZM. On-line monitoring of contrast agent arterial input function in mouse MRI. Proc Intl Soc Mag Reson Med 2002; 10: 312.
12. Graumann R, Deimling M, Heilmann T et al. A new method for fast and precise T1 determination. Proc Soc Magn Reson Med 1986; 922–923.
13. Brix G, Schad LR, Deimling M, et al. Fast and precise T1 imaging using a TOMROP sequence. Magn Reson Imag 1990; 8:351–356.
14. Levitt MH, Di Bari L. Steady state in magnetic resonance pulse experiments. Phys Rev Lett 1992; 69:3124–3127.
15. Zhou R, Pickup S, Glickson JD, et al. Assessment of global and regional myocardial function in the mouse using cine and tagged MRI. Magn Reson Imag 2003; 49:760–764.
16. Donahue KM, Burstein D, Manning WJ, et al. Studies of Gd-DTPA relaxivity and proton exchange rates in tissue. Magn Reson Imag 1994; 32:66–76.
17. Doyle M, Walsh EG, Foster RE, et al. Rapid cardiac imaging with turbo BRISK. Magn Reson Med 1997; 37:410–417.
18. Sodickson DK, Manning WJ. Simultaneous acquisition of spatial harmonics (SMASH): Fast imaging with radiofrequency coil arrays. Magn Reson Med 1997; 38:591–603.
19. Sodickson DK, Griswold MA, Jakob PM, et al. Signal-to-noise ratio and signal-to-noise efficiency in SMASH imaging. Magn Reson Med 1999; 41:1009–1022.
20. Wang Y. Description of parallel imaging in MRI using multiple coils. Magn Reson Med 2000; 44:495–499.
21. Zhou R, Pickup S, Yankeelov T, et al. Simultaneous measurement of arterial input function and tumor perfusion in mice. Proc ISMRM Workshop on In Vivo Functional and Molecular Assessment of Cancer, Santa Cruz, California, 2002; 8–9.
22. Weinmann HJ, Brasch RC, Press WR, Wesbey GE. Characteristics of gadolinium-DTPA complex: A potential NMR contrast agent. Am J Rad 1983; 142:619–24.